Self-pulsing and chaos in short chains of coupled nonlinear microcavities

Bjorn Maes,* Martin Fiers, and Peter Bienstman
Photonics Research Group (INTEC), Ghent University–IMEC, Sint-Pietersnieuwstraat 41, B-9000 Ghent, Belgium
(Received 16 June 2009; published 2 September 2009)

We examine time-domain instabilities in short chains of coupled Kerr-nonlinear resonators. We show that a large parameter region of self-pulsing or chaotic behavior can be realized. We give a detailed description of the possible states in systems with two and three cavities, using phenomenological coupled-mode equations and rigorous simulations. A particular geometry can exhibit a rich range of dynamics, dependent on input conditions. A clear link with the linear transmission properties is shown. This system complements the studies of the nonlinear Bragg reflector and electrons in a nonlinear lattice. Unlike the Bragg grating case, we observe wide detuning ranges that exhibit self-pulsing without first going through a bistable transition.

DOI: 10.1103/PhysRevA.80.033805 PACS number(s): 42.65.Sf, 42.65.Pc

I. INTRODUCTION

Currently, two interesting evolutions take place with an impact on nonlinear integrated photonics. First, experimenters have fabricated complex designs that integrate multiple consecutive resonators [1,2]. Second, novel material systems are characterized, which exhibit a strong and pure Kerr-like behavior, e.g., with negligible two-photon absorption. In particular, we note chalcogenide materials [3] and hybrid systems, e.g., silicon with a nonlinear organic material deposited on top [4]. In this paper, we combine these two trends: we examine the nonlinear behavior of connected Kerr resonators, with a focus on temporal instabilities.

To initiate this research and keep the results tractable, we focus first on short chains of resonators. We study these systems for the appearance of time-domain instabilities, as indeed the temporal behavior is not as well examined as the frequency domain characteristics. In addition, the small number of resonators makes the structures more accessible for near-term experiments. As possible implementations, we consider nonlinear photonic crystal cavities, as they have proven to be viable experimental systems [5–7]. However, the model that we employ is more general, so it also applies to ring resonators or Bragg cavities.

The study of temporal instabilities is important as it mimics the behavior in experiments [8]. In contrast to Fabry-Pérot cavities, one does not consider transverse instabilities in the localized integrated cavities. However, there is a host of other destabilizing mechanisms, even in a single cavity [9]. A known phenomenon is the oscillating behavior when competing nonlinearities with different signs and time scales are present in the system [10–12]. Indeed, in semiconductors such as silicon, the nonlinearity is quite complex because of carrier dynamics. Possibilities for interesting dynamics show up with resonant nonlinearities [13] or when different frequencies interact during second-harmonic or third-harmonic generation [14].

In this paper, we are particularly interested in the appearance of self-pulsing or chaos. In both cases, a constant input signal leads to a time-varying output signal, which is periodic or chaotic, respectively. The model equations in our system lead to the discrete nonlinear Schrödinger equation (DNLS). In the transmission problem that we examine, this means that we study the driven DNLS [15]. The appearance of self-pulsing and chaotic dynamics is well known in these kinds of systems. However, it was not well studied in this particular geometry. In addition, it was not mapped what the interesting regions would be for a small number of cavities, which are most relevant for experiments. Indeed, the literature mostly focuses on a large number of equations, as these models stem from the study of multilayer systems without defects.

The study of temporal instabilities in nonlinear distributed Bragg reflectors [16–18] has a particular correspondence to the present study. Pulsing and chaos have theoretically been described [19–21]: the oscillating output is explained by the movement of a localized nonlinear excitation, or gap soliton, from the front to the back. This temporal behavior or convective process was also described in [22].

These optical studies have complemented the study of electrons in a nonlinear lattice [23,24], which are modeled by similar equations. In these papers, a nonlinear dynamical approach was used, which linked important features in the transmission problem to periodic solutions of an iterated map.

In contrast to previous studies [17], we look closer into the chaotic behavior of these systems, as such dynamics can be very useful for integrated random bit generators [25] or secure chaos-encoded optical communications [26].

The paper is structured as follows. First we describe the model equations and, in the two subsequent sections, we examine in detail chains with two and three resonators, respectively. Next we show the validity of the model and the effects by a comparison with rigorous finite-difference time-domain (FDTD) simulations on a two-dimensional (2D) photonic crystal structure. For these simulations, we employ MEEP, a freely available software package with subpixel smoothing for increased accuracy [27].

II. MODEL

The particular system under study is a chain of cavities, which are coupled by waveguide sections. As shown in Fig.

*bjorn.maes@ugent.be

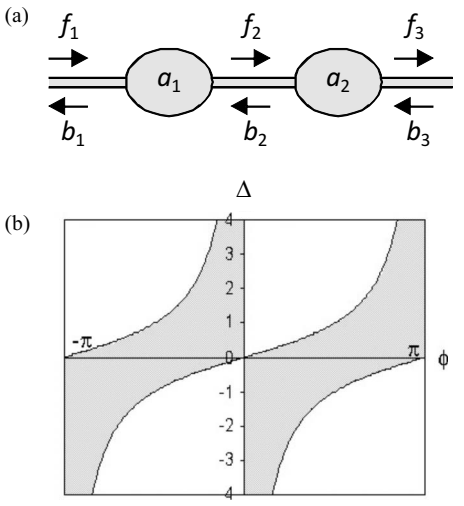

FIG. 1. (a) A schematic representation of two cavities. (b) Bloch modes of the infinite structure; transmissive bands are shaded.

1(a), the resonators block the waveguide [28]. To model this geometry, we employ the coupled-mode theory (CMT) as developed by Haus and co-workers [29]. Because we use this generic model, the observed phenomena are quite general.

For each section, we have the following equations [30,31]:

$$\frac{da_j}{dt} = \left[i(\omega_0 + \delta\omega_j) - \frac{1}{\tau} \right] a_j + df_j + db_{j+1}, \tag{1}$$

$$b_j = \exp(i\phi) f_j + da_j, \tag{2}$$

$$f_{j+1} = \exp(i\phi) b_{j+1} + da_j, \tag{3}$$

for $j=1,\ldots,N$; with N as the number of cavities. Here $d = i\exp(i\phi/2)/\sqrt{\tau}$, where τ is the lifetime of the cavity and ϕ represents the phase that depends on the waveguide length and the resonator mirror reflection properties. The nonlinear frequency shift is $\delta\omega_j = -|a_j|^2/(P_0\tau^2)$, with P_0 the "characteristic nonlinear power" of the cavity [28]. In these equations, $|a_j|^2$ is the energy in the cavity mode. $|f_j|^2$ (respectively, $|b_j|^2$) represents the power flowing in the (single-mode) waveguide in the forward (respectively, backward) direction. Thus, $|f_1|^2 \equiv P_{in}$ is the input power, and $|f_{N+1}|^2 \equiv P_{trans}$ is the transmitted power. We assume no input from the right, $b_{N+1}=0$. In this paper, we will mainly limit ourselves to $N \leq 3$.

The previous system is equivalent to a driven DNLS. To show this structure, we eliminate the internal waveguide amplitudes from Eqs. (1)–(3) and obtain for $N=3$,

$$\frac{da_1}{dt} = \left\{ i\Delta_1 - \frac{1}{2\tau}[i\cot(\phi) + 1] \right\} a_1 + df_1 + \kappa a_2, \tag{4}$$

$$\frac{da_2}{dt} = \left[i\Delta_2 - \frac{i\cot(\phi)}{\tau} \right] a_2 + \kappa a_1 + \kappa a_3, \tag{5}$$

$$\frac{da_3}{dt} = \left\{ i\Delta_3 - \frac{1}{2\tau}[i\cot(\phi) + 1] \right\} a_3 + \kappa a_2, \tag{6}$$

with $\Delta_j = \omega_0 + \delta\omega_j$, for $j=1,2,3$. Here $\kappa = -i/(2\tau\sin\phi)$. Note how the coupling to the input and output external waveguides is given by the $1/(2\tau)$ loss term in Eqs. (4) and (6). For $N>3$, we simply have more equations like the middle one [Eq. (5)]. In this way, we immediately link our study to the extensive knowledge of the DNLS [15].

Although we discuss short finite structures, it is important to review the Bloch modes of the infinite linear system, which allows us to divide the parameter space into transmissive and blocking bands [31]. The results are shown in Fig. 1(b). In this paper, we define the dimensionless detuning as $\Delta = \tau(\omega - \omega_0)$. We see that the band edges strongly depend on the phase ϕ, and this parameter will also have a strong influence on the dynamics, as discussed later.

We employ the conventional method to solve Eqs. (1)–(3) for nonlinear steady-state ($da_j/dt=0$) solutions: one starts from a chosen P_{trans} at the end and propagates toward the beginning. To assess the stability and its nature, we employ linear stability analysis, so we examine the eigenvalues of the Jacobian. If all eigenvalues have negative real part, the solution is stable. If there is an eigenvalue with positive real part, this solution will evolve toward other states. If the unstable eigenvalue is real, we expect a steady evolution toward another state. There is also the possibility of an unstable complex-conjugate pair. This leads to oscillatory behavior and can result in a stable limit cycle or periodic solution: the system exhibits self-pulsing. Apart from self-pulsing, there is also the possibility of chaos. To examine in more detail which state the system will evolve into, we calculate the time-dependent equations by using an ordinary differential equation solver [32].

The case of a single cavity with input from one side and pure Kerr nonlinearity is well known. At sufficient detuning, the output versus input power has the typical bistable S shape [28]. The unstable part is the negative slope section between the twofolding points. These states will evolve into the upper or lower *stable* branches, so we do not examine these transient dynamics here.

III. TWO CAVITIES

We now examine the two-cavity case. From the previous section, we notice that the steady-state solutions of our model equations can be determined by three parameters: the transmitted power P_{trans}, the phase ϕ, and the detuning Δ. Therefore, to get an overview of the possible states of the system we plot the transmission $T = P_{trans}/P_{in}$ in a graph of P_{trans} versus Δ, at a constant ϕ. In addition, we divide the regions into the possible dynamics. (i) Stable: all eigenvalues of the linear stability analysis have negative real part; (ii) bistable: there is an unstable eigenvalue which is positive and real; (iii) self-pulsing: a complex-conjugate pair exists with positive real part; and (iv) chaos. The "bistable" regions correspond to the aforementioned instability in single cavities: the negative slope parts that evolve to the stable upper or lower branches.

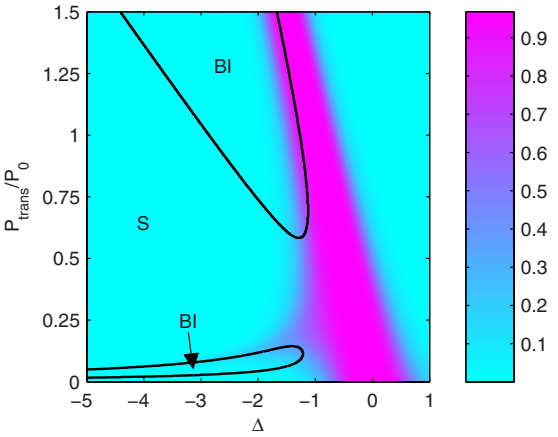

FIG. 2. (Color online) Transmission and classification of the two-cavity device for $\phi=0.5\pi$: (S) stable; (BI) bistable.

The chaotic solutions are inside the self-pulsing regions. To distinguish between periodic and chaotic solutions, we determine the maximal Lyapunov exponent numerically. We employed MATLAB code built on an implementation by Govorukhin, which uses an established algorithm [33]. For a stable periodic solution, the maximal Lyapunov exponent is zero, for a chaotic solution this exponent is larger than zero. Numerically, we employed a threshold of 1.5×10^{-4} to distinguish the two types of behavior.

An example of results for two cavities and $\phi=0.5\pi$ is shown in Fig. 2. For this particular phase ϕ, we do not observe self-pulsing and chaos. In effect, this graph looks very similar to the single cavity case, with a large bistable window opening up at sufficient detuning and transmitted power. However, there is a difference at the narrow bistable region for small $P_{trans}(\approx 0.1P_0)$. This is a first indication of gap solitonlike effects: states, or resonant trajectories, which move into the linear gap [34]. Here the transmission quickly drops, so the effect is not fully evolved. This suggests that the structure does not accommodate solitons well.

For two cavities, more interesting results show up at other ϕ values (see Fig. 3 for $\phi=0.2\pi$). A substantial self-pulsing region shows up. There is also the possibility of chaos, as

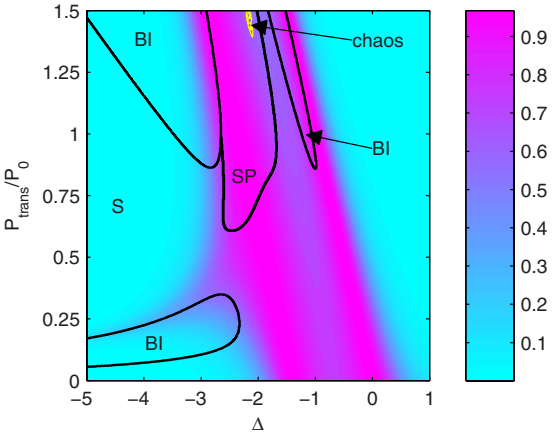

FIG. 3. (Color online) Transmission and classification of the two-cavity device for $\phi=0.2\pi$: (S) stable, (BI) bistable, and (SP) self-pulsing and chaos.

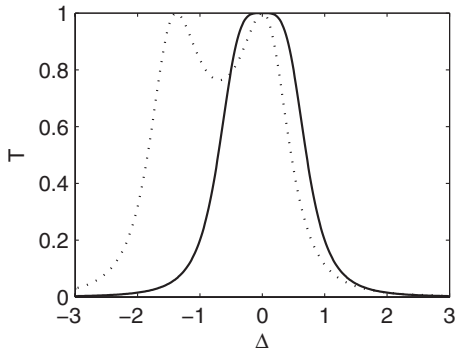

FIG. 4. Linear transmission T versus Δ of the two-cavity series with $\phi=0.5\pi$ (solid) and $\phi=0.2\pi$ (dotted), respectively.

visible by the small region in Fig. 3 around $P_{trans}/P_0=1.45$ and $\Delta=-2.15$. So in this structure and parameter region, the chaos is limited.

It is interesting to note that in many systems, the nonlinear effects are most effective when the phase corresponds to $\lambda/4$ or $\pi/2$ [35]. For example, this often leads to switching with the lowest power [36]. On the other hand, in this particular case with two cavities, the dynamics are limited at $\phi=0.5\pi$. This becomes clearer when we examine the linear transmission (see Fig. 4): for $\phi=0.5\pi$, the transmission peaks coalesce into one broader peak, rendering it similar to the one-cavity case. For $\phi=0.2\pi$, the two transmission peaks are separate.

The previous linear transmission discussion also provides more insight into the nonlinear behavior. The main feature in Fig. 3 for the transmission is the shift of the two transmission peaks to more negative detunings, as P_{trans} increases. These two peaks explain the two bistable regions starting at $P_{trans}\approx 0.85P_0$, similar to the single cavity (and thus single peak) case. Similar to $\phi=0.5\pi$, there is a bistable region at smaller P_{trans} related to gap solitons moving into the gap. The most interesting region here is the self-pulsing area. Unlike the case of the Bragg grating [17], there is a wide range of detunings ($\Delta=-2.4$ to -1.6), where self-pulsing is reachable without first going through a bistable jump.

The previous regimes are reflected in the nonlinear characteristics of P_{trans} versus P_{in} shown in Fig. 5. For $\Delta=-3$, we observe two bistable regions. For $\Delta=-1.2$, we have a single bistable region, and this characteristic also shows the strong limiting behavior possible in these structures [23]. This limiting stems from the shifting of the transmission peaks past the operating detuning. Both $\Delta=-2$ and -3 show unstable regions with positive slope. More specifically, in these regions there is a complex-conjugate pair of unstable eigenvalues. This leads to self-pulsing, which is proven by the time-domain results.

Some time-domain examples are illustrated in Fig. 6, where we assume that the input switches on at $t=0$ as a step function. The self-pulsing is clear for $\Delta=-2$ and $P_{in}/P_0=1.0$ (dash-dotted blue line). The solution in solid red in Fig. 6, corresponding with $\Delta=-3$ and $P_{in}/P_0=2.0$, illustrates an important aspect of the time-domain calculations. We do not know *a priori* which behavior a certain input power will result in, when there are multiple solutions possible in the

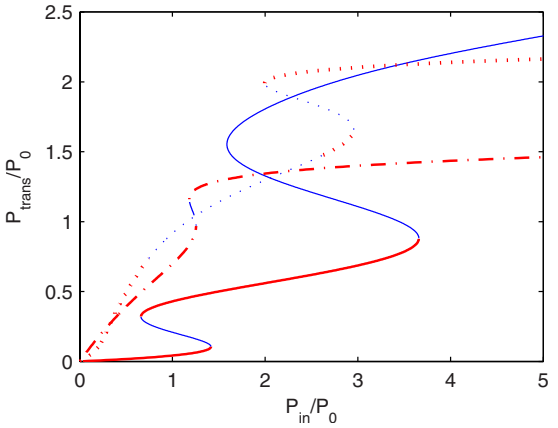

FIG. 5. (Color online) P_{trans} versus P_{in} nonlinear characteristics for two cavities at $\phi=0.2\pi$ with $\Delta=-3$ (solid), $\Delta=-2$ (dotted), and $\Delta=-1.2$ (dash-dotted). Stable (unstable) solutions are in thicker red (thin blue).

continuous-wave (cw) characteristic. Indeed in Fig. 5 for $\Delta=-3$ and $P_{in}/P_0=2.0$, we observe a stable solution and two unstable solutions, the top one of which has pulsing properties. In the time series, we indeed see that at the beginning there are oscillations, meaning that the system approaches the self-pulsing solution. In the end, however, the system does settle on the constant stable solution. This is the result for a step-function input. Other solutions may be reached by different inputs.

The self-pulsing period can be estimated by the imaginary part of the unstable eigenvalue from the linear stability analysis [17]: period$=2\pi/\mathrm{Im}$(eigenvalue). As an example, the oscillating solution of Fig. 6 provides us with a period of 7.69τ, whereas the eigenvalue gives 7.65τ. The approximation is better if the particular oscillating solution is closer to the onset of instability.

IV. THREE CAVITIES

For three cavities, the behavior becomes more intricate. We map the situation for $\phi=0.5\pi$ in Fig. 7. In this case, the

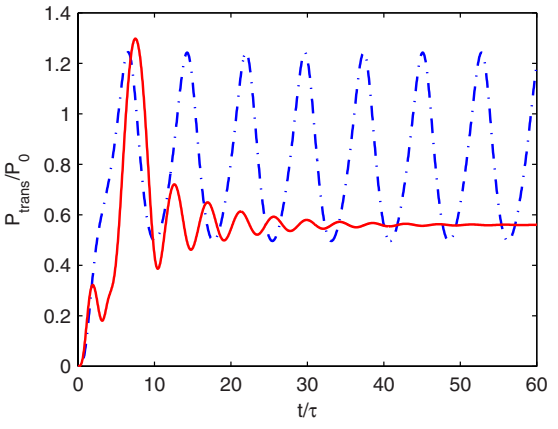

FIG. 6. (Color online) Time-domain solutions for two cavities with $\phi=0.2\pi$ with $\Delta=-2$ and $P_{in}/P_0=1.0$ (blue dash-dotted line) and $\Delta=-3$ and $P_{in}/P_0=2.0$ (red solid line).

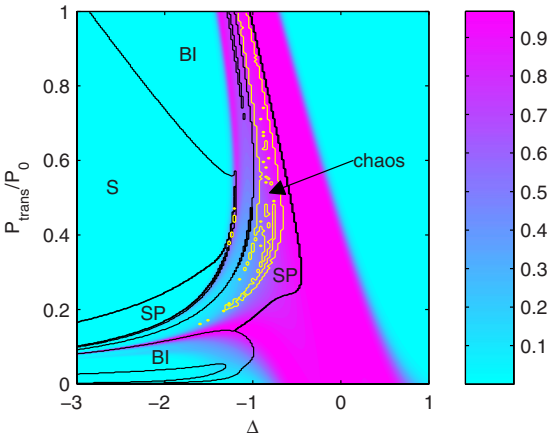

FIG. 7. (Color online) Transmission and classification of the three-cavity device for $\phi=0.5\pi$: (S) stable, (BI) bistable, and (SP) self-pulsing and chaos (bounded by thin yellow line).

linear transmission consists of three peaks that are closest together at this phase but still distinguishable (see Fig. 8). We notice in Fig. 7 a clear detachment of one of the transmission peaks into the linear gap region, which corresponds to gap solitonlike behavior [34].

Similar to the two-cavity case at $\phi=0.2\pi$, there is a substantial region with self-pulsing behavior. A narrow second region of self-pulsing is visible in the gap. For three cavities, in this parameter range, there is a significantly larger possibility for chaos compared to two cavities. Before the onset of chaos, period doubling is observed in the time-domain calculations. We notice in Fig. 7 that the domain with chaos has a very complex boundary, with regions of regular self-pulsing inside.

Typical P_{trans} versus P_{in} curves are shown in Fig. 9. For $\Delta=-0.5$, a clear self-pulsing region is available, without bistable transitions. At larger detunings, such as $\Delta=-1.0$, the curve becomes more complex and shows a number of different regions. The (two) negative slope regions correspond with the nonoscillating instability; the (two) positive slope unstable regions correspond with self-pulsations or chaos. In these cases with multistability, the time-domain behavior is harder to predict and control.

This is illustrated by the time-domain results of Fig. 10. For $\Delta=-0.5$, the self-pulsing solutions are regular, nearly

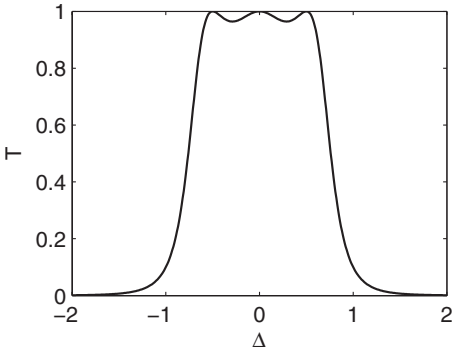

FIG. 8. Linear transmission T versus detuning Δ for three cavities with $\phi=0.5\pi$.

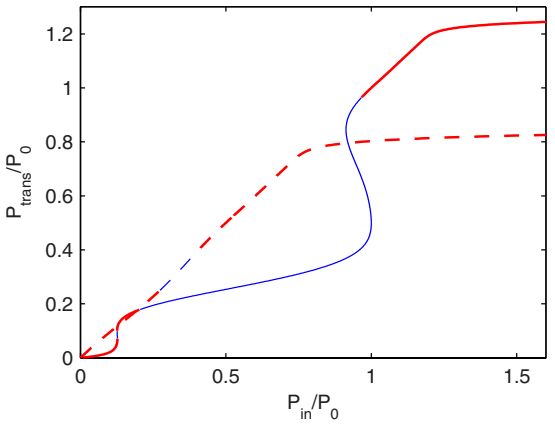

FIG. 9. (Color online) P_{trans} versus P_{in} nonlinear characteristics for three cavities at $\phi=0.5\pi$ with $\Delta=-1$ (solid) and $\Delta=-0.5$ (dashed). Stable (unstable) solutions are in thicker red (thin blue).

sinusoidal. For $\Delta=-1$, the solutions become more complex, interesting periodic, and chaotic behavior is observed.

The self-pulsing behavior in systems such as Bragg reflectors has been linked with the movement of gap solitons through the structure from input to output facet [20]. Although our structures are too short to fully exhibit this kind of convective movement, we do observe that during self-pulsing the maximum cavity strength moves from input to output cavity. This suggests that similar ideas apply, even for the very short chains. This is also suggested by a slightly longer period for the three-cavity case (9.5τ, blue solution in Fig. 10) compared to the two-cavity case (7.69τ, Fig. 6).

V. FDTD SIMULATIONS

To validate the results found with CMT, we compare them with rigorous FDTD simulations of a 2D photonic crystal, by extending the geometry in [28] (see Fig. 11). The lattice is rectangular (lattice constant a) and consists of circular rods with refractive index $n_{high}=3.5$ placed in a lower refractive index medium $n_{low}=1.5$. The rods have a radius $r=0.25a$. We can make a line defect by reducing the radius of the rods to

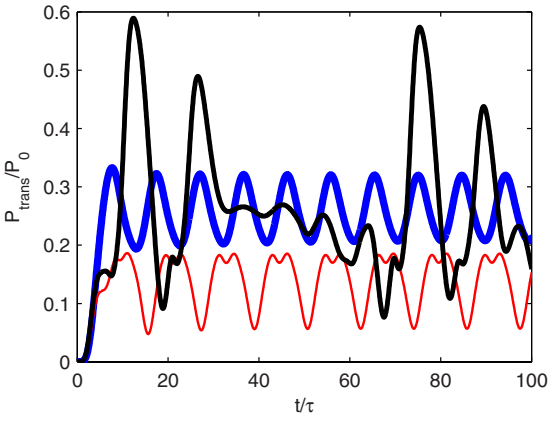

FIG. 10. (Color online) Time-domain solutions for three cavities with $\phi=0.5\pi$ with $\Delta=-0.5$ and $P_{in}/P_0=0.3$ (thick blue) and $\Delta=-1$ for $P_{in}/P_0=0.4$ (thin red) and $P_{in}/P_0=0.55$ (medium black).

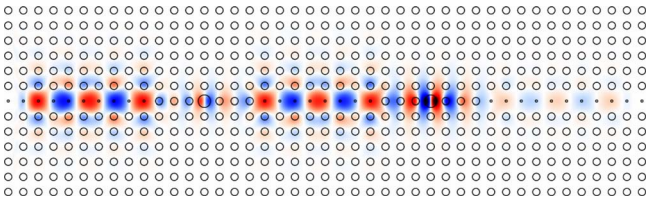

FIG. 11. (Color online) Geometry of a two-cavity device and example of an electric field plot with FDTD.

$r/3$, which creates a waveguide. We can also make a point defect inside the waveguide, by increasing the radius to $5r/3$, surrounded by three normal rods. This creates a resonant cavity. The center point defect has a pure Kerr nonlinearity with coefficient n_2. The simulation domain is terminated by a perfectly matched layer (PML) of thickness $2a$ on the left and right. The unit cell is discretized by 36×36 pixels, which is enough for convergence. The normalized frequency ω_{norm} is defined as $\omega=\omega_{norm}(2\pi c/a)$. In the following discussion, we will always use ω_{norm}. The structure is excited with TM-polarized light (one transversal electric field component). For this polarization, there is a photonic band gap from $\omega=0.2424$ to 0.2897.

To find the resonance of the cavity, we launch a low-power broad pulse ($\omega=0.2615$, $\Delta\omega=0.008$) into the waveguide. The cavity is designed to have a transmission with a Lorentzian shape $T(\omega)=\gamma^2/[\gamma^2+(\omega-\omega_{res})^2]$. In this way, we find $\omega_{res}=0.262087$, and a Q factor of roughly $\omega_{res}/(2\gamma)\approx400$.

We model the bistable behavior by using cw signals at a frequency $\omega=0.261\,298$. To reach the bistable section of the upper branch of the curve, we inject an extra initial pulse together with the cw signal [28]. From Fig. 12, we see a good agreement with the theoretical curve [28],

$$\frac{P_{trans}}{P_{in}}=\frac{1}{1+(P_{trans}/P_0-\Delta)^2} \tag{7}$$

for $\Delta=-3.4411$. The specific value of P_0 depends on the used n_2. For a realistic value $n_2=1.5\times10^{-5}$ $\mu m^2/W$ in this geometry, it has been shown that P_0 can be brought below 77 mW [28].

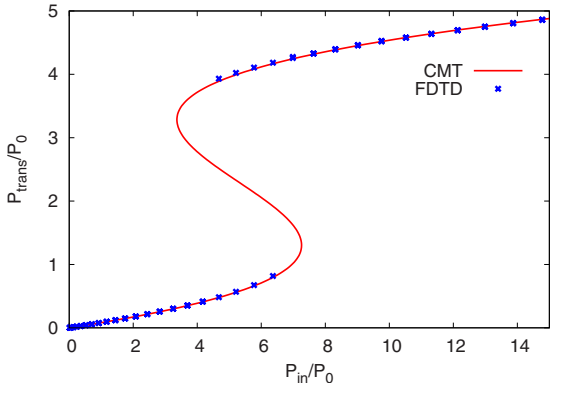

FIG. 12. (Color online) Simulations of one cavity. The crosses represent FDTD simulations; the full line shows CMT results.

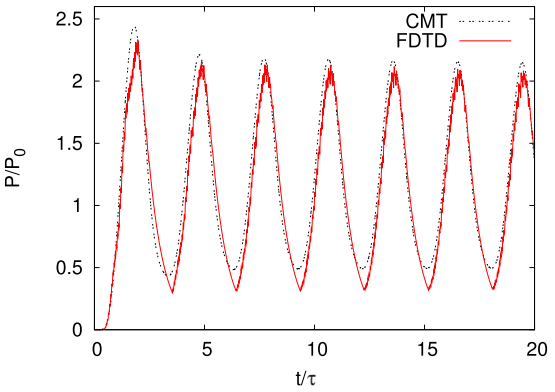

FIG. 13. (Color online) Resulting time signal of P_{trans} for the parameters described in the text. The dotted black line shows CMT; the red line is the FDTD result.

When we couple two cavities, we get an extra degree of freedom: the number of rods between the two cavities. This determines the phase ϕ and greatly influences the dynamics of the chain. For 14 rods between the centers of the two cavities (see Fig. 11), we obtain self-pulsing. We obtain the value of ϕ by comparing the linear transmission with FDTD and CMT and get $\phi \approx 0.231$.

For these parameter values, CMT predicts the component to start self-pulsing at around $P_{in}/P_0=5.52$. The exact power at which self-pulsing starts is difficult to determine with FDTD as there can be a slow damping of the oscillations. Therefore, we use a slightly larger $P_{in}/P_0=5.6254$. In addition, the exact time signal is quite sensitive to small parameter variations. However, as can be seen in Fig. 13, we observe self-pulsing both in CMT and FDTD, and there is a good quantitative agreement for $\phi=0.2333$.

VI. CONCLUSIONS

We have studied small numbers of resonators, which corresponds with experimentally reachable situations. To our knowledge, these self-pulsing effects with pure Kerr nonlinearity have not been observed yet in integrated coupled cavity devices. Our results show that the system with two or more coupled cavities could readily provide self-pulsing behavior. In contrast with Bragg gratings, there are ranges of frequencies where self-pulsing is reachable without undergoing a bistable jump.

In addition, we have mapped that chaos is quite common at low powers with three cavities. This could prove useful for integrated random bit generators [25] or chaos communications [26]. Furthermore, the region between a few and a larger number of resonators [31] still needs to be explored. These optical systems inherently have a lot of control opportunities, which can help in the general study of turbulent systems. Finally, networks like the ones presented here could be viable for an optical realization of reservoir computing [37].

ACKNOWLEDGMENTS

We are grateful to Yuri Kivshar for useful discussions. This work is supported by COST Action MP0702 and the interuniversity attraction pole (IAP) Photonics@be of the Belgian Science Policy Office. B.M. acknowledges the Research Foundation-Flanders. M.F. acknowledges the Special Research Fund. Computational resources and services were provided by Ghent University.

[1] F. Xia, L. Sekaric, and Y. Vlasov, Nat. Photonics **1**, 65 (2007).
[2] M. Notomi, E. Kuramochi, and T. Tanabe, Nat. Photonics **2**, 741 (2008).
[3] M. Galili, J. Xu, H. C. H. Mulvad, L. K. Oxenlowe, A. T. Clausen, P. Jeppesen, B. Luther-Davies, S. Madden, A. Rode, D.-Y. Choi *et al.*, Opt. Express **17**, 2182 (2009).
[4] C. Koos, P. Vorreau, T. Vallaitis, P. Dumon, W. Bogaerts, R. Baets, B. Esembeson, I. Biaggio, T. Michinobu, F. Diederich *et al.*, Nat. Photonics **3**, 216 (2009).
[5] P. E. Barclay, K. Srinivasan, and O. Painter, Opt. Express **13**, 801 (2005).
[6] M. Notomi, A. Shinya, S. Mitsugi, G. Kira, E. Kuramochi, and T. Tanabe, Opt. Express **13**, 2678 (2005).
[7] T. Uesugi, B. S. Song, T. Asano, and S. Noda, Opt. Express **14**, 377 (2006).
[8] H. M. Gibbs, F. A. Hopf, D. L. Kaplan, and R. L. Shoemaker, Phys. Rev. Lett. **46**, 474 (1981).
[9] A. E. Miroshnichenko, Y. S. Kivshar, C. Etrich, T. Pertsch, R. Iliew, and F. Lederer, Phys. Rev. A **79**, 013809 (2009).
[10] H. M. Gibbs, *Optical Bistability: Controlling Light with Light* (Academic Press, New York, 1985).
[11] G. Priem, P. Dumon, W. Bogaerts, D. Van Thourhout, G. Morthier, and R. Baets, Opt. Express **13**, 9623 (2005).
[12] T. J. Johnson, M. Borselli, and O. Painter, Opt. Express **14**, 817 (2006).
[13] P. V. Paulau and N. A. Loiko, Phys. Rev. A **72**, 013819 (2005).
[14] Hila Hashemi, Alejandro W. Rodriguez, J. D. Joannopoulos, Marin Soljacic, and Steven G. Johnson, Phys. Rev. A **79**, 013812 (2009).
[15] D. Hennig and G. P. Tsironis, Phys. Rep. **307**, 333 (1999).
[16] C. M. de Sterke, Phys. Rev. A **45**, 8252 (1992).
[17] A. Parini, G. Bellanca, S. Trillo, M. Conforti, A. Locatelli, and C. De Angelis, J. Opt. Soc. Am. B **24**, 2229 (2007).
[18] B. Eggleton, C. de Sterke, A. Aceves, J. Sipe, T. Strasser, and R. Slusher, Opt. Commun. **149**, 267 (1998).
[19] H. G. Winful and G. D. Cooperman, Appl. Phys. Lett. **40**, 298 (1982).
[20] C. M. de Sterke and J. E. Sipe, Phys. Rev. A **42**, 2858 (1990).
[21] D. Pelinovsky and E. H. Sargent, J. Opt. Soc. Am. B **19**, 1873 (2002).
[22] F. Geniet and J. Leon, Phys. Rev. Lett. **89**, 134102 (2002).
[23] F. Delyon, Y. E. Levy, and B. Souillard, Phys. Rev. Lett. **57**, 2010 (1986).
[24] Y. Wan and C. M. Soukoulis, Phys. Rev. A **41**, 800 (1990).

[25] A. Uchida, K. Amano, M. Inoue, K. Hirano, S. Naito, H. Someya, I. Oowada, T. Kurashige, M. Shiki, S. Yoshimori *et al.*, Nat. Photonics **2**, 728 (2008).
[26] A. Argyris, M. Hamacher, K. E. Chlouverakis, A. Bogris, and D. Syvridis, Phys. Rev. Lett. **100**, 194101 (2008).
[27] A. Farjadpour, D. Roundy, A. Rodriguez, M. Ibanescu, P. Bermel, J. D. Joannopoulos, S. G. Johnson, and G. W. Burr, Opt. Lett. **31**, 2972 (2006).
[28] M. Soljacic, M. Ibanescu, S. G. Johnson, Y. Fink, and J. D. Joannopoulos, Phys. Rev. E **66**, 055601(R) (2002).
[29] C. Manolatou, M. Khan, S. H. Fan, P. R. Villeneuve, H. A. Haus, and J. D. Joannopoulos, IEEE J. Quantum Electron. **35**, 1322 (1999).
[30] S. H. Fan, W. Suh, and J. D. Joannopoulos, J. Opt. Soc. Am. A Opt. Image Sci. Vis **20**, 569 (2003).
[31] B. Maes, P. Bienstman, and R. Baets, J. Opt. Soc. Am. B **22**, 1778 (2005).
[32] E. Jones, T. Oliphant, and P. Peterson (www.scipy.org) (2001).
[33] A. Wolf, J. B. Swift, H. L. Swinney, and J. A. Vastano, Physica D **16**, 285 (1985).
[34] E. Lidorikis, Q. M. Li, and C. M. Soukoulis, Phys. Rev. B **54**, 10249 (1996).
[35] S. Radic, N. George, and G. P. Agrawal, Opt. Lett. **19**, 1789 (1994).
[36] B. Maes, P. Bienstman, and R. Baets, Opt. Express **16**, 3069 (2008).
[37] K. Vandoorne, W. Dierckx, B. Schrauwen, D. Verstraeten, R. Baets, P. Bienstman, and J. Van Campenhout, Opt. Express **16**, 11182 (2008).